Mach Reflection Flowfields Associated with Strong Shocks

Harold Mirels*
The Aerospace Corporation, El Segundo, California

The Mach reflection associated with the passage of a shock wave over a wedge is treated in the limit of an ideal gas and a strong shock. In this limit, flow properties are functions only of wedge angle θ and the ratio of specific heats γ. Numerical results are presented for $\gamma = 9/7$, 7/5, and 5/3. Wedge angles are noted at which the transition from regular to double-, complex-, and simple-Mach reflection occurs. Characteristic velocities in the recirculation region associated with double-Mach reflection are estimated. Local surface pressure maxima at the upstream and downstream edges of the recirculation region are also estimated. The scale of the recirculation region increases with decreases in γ, in accord with experimental observations. The present results provide a convenient characterization of Mach reflection flowfields associated with wedge flows.

Introduction

THE passage of a shock wave over a wedge results in either a regular or Mach reflection. A regular reflection (RR) occurs when the wedge angle is large. With decrease in wedge angle, the reflection of a strong shock becomes, successively, a double- (DMR), complex- (CMR), and single-Mach (SMR) reflection. These flows are illustrated in Fig. 1. The DMR is characterized by two Mach stems (m and m' in Fig. 1b) whereas the CMR is characterized by a "kink" in the reflected wave (K in Fig. 1c). The wedge angles at which flowfield transitions occur, and the nature of the DMR and CMR flowfields, have been studied experimentally and analytically in, for example, Refs. 1-4. Results from Ref. 4 are included in Fig. 2 and are discussed later. It is seen from Fig. 2 that the DMR and CMR flowfields occur only with relatively strong incident shocks (e.g., $M_i \gtrsim 3$ for CO_2) and it is only in recent years that these flows have been examined in detail.[1-4]

The flowfield associated with a DMR is further illustrated in Fig. 3. Flow properties in regions 1-3 can be found by classical methods if it is assumed that the primary Mach stem m is straight and perpendicular to the wedge surface (e.g., Refs. 2 and 3). The flows in regions 4 and 5 are less well characterized. A knowledge of characteristic surface pressures and flow velocities in regions 4 and 5 is needed for estimating blast effects on ground structures. Computer codes have been developed which describe the DMR flowfield (e.g., Ref. 5), but these are expensive to operate. Also, the codes generally require a compromise between run time and mesh size which tends to smear out details of the flow.

The primary purpose of the present study is to characterize the flow in DMR regions 4 and 5 by use of a simple analytic model. A strong incident shock and an ideal gas are considered. In this limit, flow properties are functions only of wedge angle θ and the ratio of specific heats, γ. Regular as well as Mach reflections are considered and flow properties of interest are tabulated for $\gamma = 9/7$, 7/5, 5/3, and a variety of wedge angles. Additional numerical results for $\gamma = 6/5$, 9/7, 7/5, and 5/3 are included in Ref. 6. These results are expected to be useful for the interpretation and correlation of experimental and numerical wedge data. The quasisteady application of wedge flows for evaluating the reflection by the ground of a strong blast wave initiated at altitude is also discussed in Ref. 6.

Received June 3, 1983; revision received April 30, 1984.

*Associate Director for Analyses, Aerophysics Laboratory. Fellow AIAA.

Discussion

Conditions across a strong shock in an ideal gas are noted in Appendix A. These are applied in Appendix B to determine the Mach reflection associated with passage of a strong shock over a wedge of angle θ. The case of regular reflection is treated in Appendix C. Numerical results presented in Tables 1-3 are discussed herein.

The flowfields are considered in a variety of coordinate systems. Velocities in laboratory coordinates are denoted u^*. Velocities in coordinate systems wherein the points T, E, and F are stationary are denoted by u, $\bar{u}$, and $\tilde{u}$. respectively, as is noted in Figs. 4 and 5. Here, point E is the intersection of the contact surface (assumed straight) with the wedge surface. Velocities in the laboratory, T, E, and F stationary coordinate systems, are related by

$$u^* = \text{laboratory} \tag{1a}$$

$$u = u^* - u_i^*/[\cos(\theta+\psi)] = \text{T stationary} \tag{1b}$$

$$\bar{u} = u - u_3 = \text{E stationary} \tag{1c}$$

$$\tilde{u} = \bar{u} - \bar{u}_m = \text{F stationary} \tag{1d}$$

where the velocities in Eqs. (1) are considered vector quantities. The symbols M_i^* and M_i are used interchangeably to denote incident shock Mach number in laboratory coordinates.

Regular Reflection

Figure 4 illustrates regular reflection in a coordinate system wherein point T is stationary. Flow properties are deduced in Appendix C and listed in Table 1.

The flow in regions 1 and 2 corresponds to supersonic flow over an equivalent wedge of angle $\delta = (\pi/2) - \beta - \theta$, as noted in Fig. 4. The oblique shock that separates regions 1 and 2 can be either weak or strong.[7] The weak-shock solution appears to be physically realistic and is used herein. The equivalent wedge angle δ increases as θ is decreased. Ultimately, a value of θ, denoted θ_D, is reached below which no oblique shock solution is possible. The transition to Mach reflection is generally assumed to occur at θ_D (i.e., shock detachment criterion). The latter criterion has been used in Fig. 2 to define the regular reflection regime. For strong shocks, θ_D depends only on γ. Numerical results for θ_D are given in Table 2.

Mach Reflection

Mach reflection flowfield properties are deduced in Appendix B. The triple-point region (regions 1-3), the criteria for the

Table 1 Regular reflection for the case of strong incident shock and ideal gas

γ	θ	M_I	β	$\frac{\rho_I}{\rho_0}$	$\frac{p_I}{M_i^2 p_0}$	M_2	δ	ω	$\frac{\rho_2}{\rho_I}$	$\frac{p_2}{p_I}$
7/5	90.00	∞	0.00	6.00	1.17	∞	0.00	0.00	3.50	8.00
	85.00	25.92	0.84	6.00	1.17	17.09	4.16	1.68	3.49	7.96
	80.00	12.87	1.68	6.00	1.17	8.40	8.32	3.43	3.47	7.84
	75.00	8.47	2.56	6.00	1.17	5.43	12.44	5.33	3.43	7.64
	70.00	6.24	3.47	6.00	1.17	3.89	16.53	7.51	3.38	7.38
	65.00	4.88	4.44	6.00	1.17	2.92	20.56	10.13	3.32	7.06
	60.00	3.95	5.50	6.00	1.17	2.22	24.50	13.53	3.25	6.73
	55.00	3.26	6.66	6.00	1.17	1.65	28.34	18.52	3.19	6.44
	50.03	2.73	7.95	6.00	1.17	0.95	32.02	32.79	3.30	6.96
5/3	90.00	∞	0.00	4.00	1.25	∞	0.00	0.00	2.50	6.00
	85.00	20.45	1.25	4.00	1.25	13.15	3.75	2.52	2.50	5.98
	80.00	10.15	2.52	4.00	1.25	6.45	7.48	5.15	2.49	5.91
	75.00	6.69	3.83	4.00	1.25	4.16	11.17	8.02	2.47	5.80
	70.00	4.94	5.20	4.00	1.25	2.97	14.80	11.34	2.45	5.66
	65.00	3.86	6.65	4.00	1.25	2.21	18.35	15.43	2.42	5.51
	60.00	3.13	8.21	4.00	1.25	1.64	21.79	21.09	2.41	5.42
	55.00	2.59	9.93	4.00	1.25	1.07	25.07	33.04	2.47	5.81
	54.66	2.56	10.05	4.00	1.25	0.95	25.29	37.25	2.53	6.21

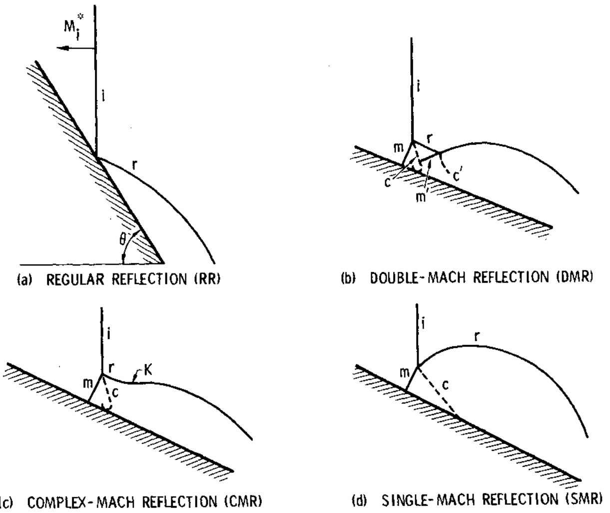

Fig. 1 Types of oblique shock-wave reflections. i = incident shock; r = reflected shock; m = Mach stem; m' = second Mach stem; K = kink; c,c' = contact surfaces (from Ref. 4).

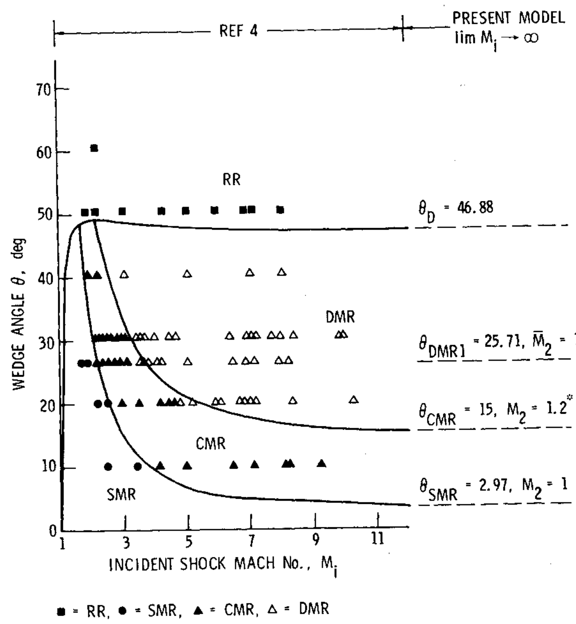

Fig. 2 Comparison of predicted reflection regions and experiment (perfect CO_2, $\gamma = 1.290$) (see Table 2).

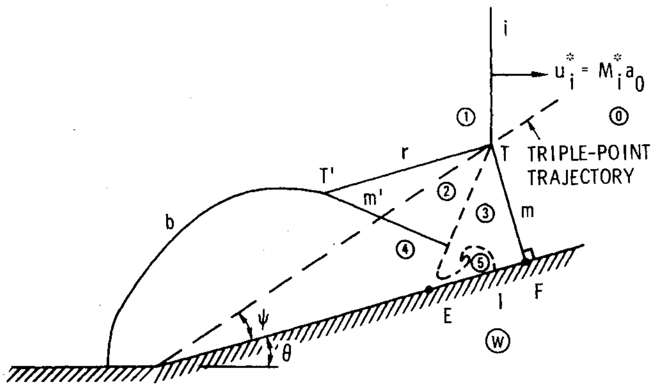

Fig. 3 Mach reflection flow regions associated with the passage of strong incident shock past wedge.

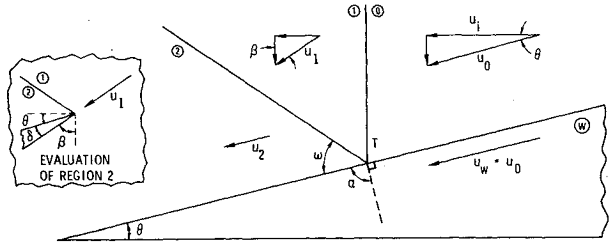

Fig. 4 Regular reflection, point T stationary.

Table 2 Wedge angles at which Mach reflection flowfield transitions occur for the case of strong shock and ideal gas

	θ			
γ	θ_D RR→DMR $M_2 > \bar{M}_2 > 1$	θ_{DMR1} $\bar{M}_2 = 1$ $M_2 \doteq 1.6$	θ_{CMR} DMR→CMR $M_2 = 1.3$	θ_{SMR} CMR→SMR $M_2 = 1$
1.10	37.34			
1.20	43.54	20.49	14.4	1.19
9/7	46.88	25.71	18.5[a]	2.97
1.30	47.34			
1.40	50.03	32.36	23.7	5.89
1.50	52.09			
1.60	53.73			
5/3	54.66	47.94	35.2	14.33

[a]Reference 4 appears to have used the value $\theta_{CMR} = 15$ deg ($M_2 = 1.2$) for $\gamma = 9/7$ (see Fig. 2).

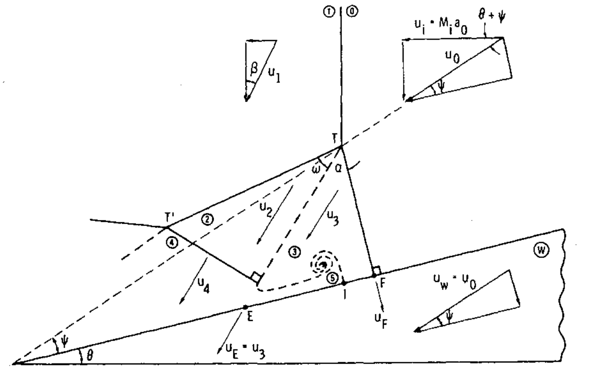

Fig. 5a Mach reflection flowfield in various coordinate systems, point T stationary.

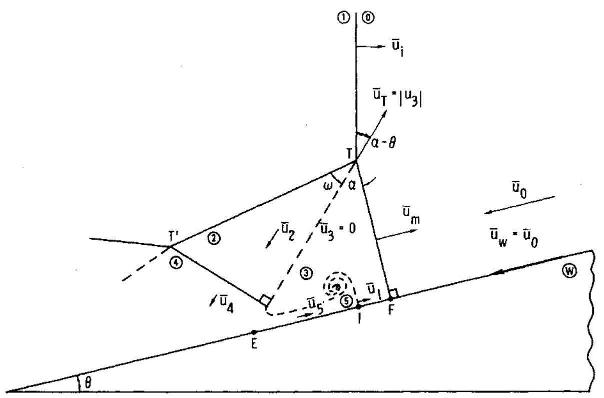

Fig. 5b Mach reflection flowfield in various coordinate systems, point E stationary.

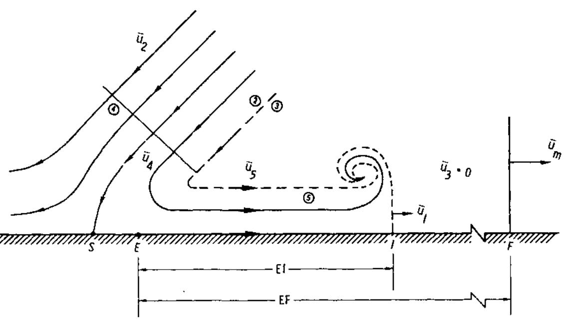

Fig. 5c Mach reflection flowfield in various coordinate systems, point E stationary (exploded view).

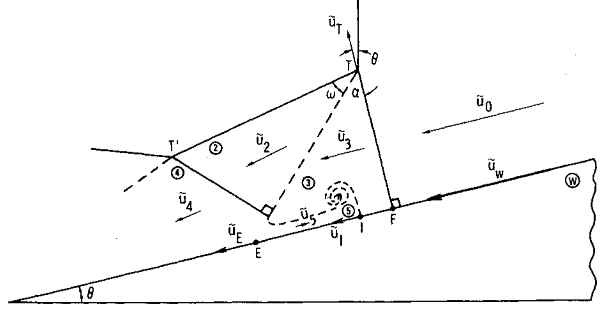

Fig. 5d Mach reflection flowfield in various coordinate systems, point F stationary.

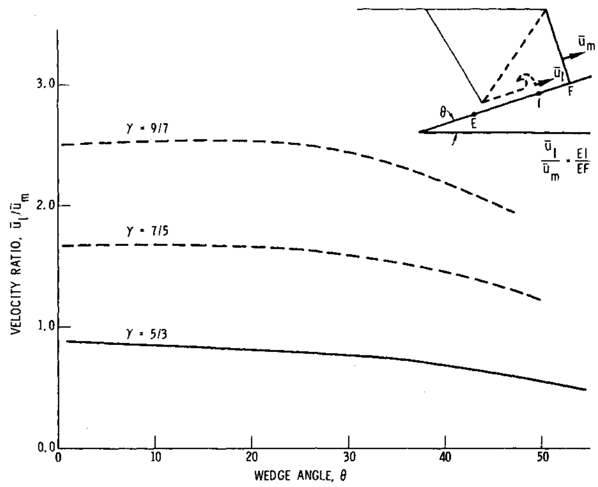

Fig. 6 Interface velocity ratio in point E stationary coordinates. Solution invalid for $(\bar{u}_I/\bar{u}_m) > 1$.

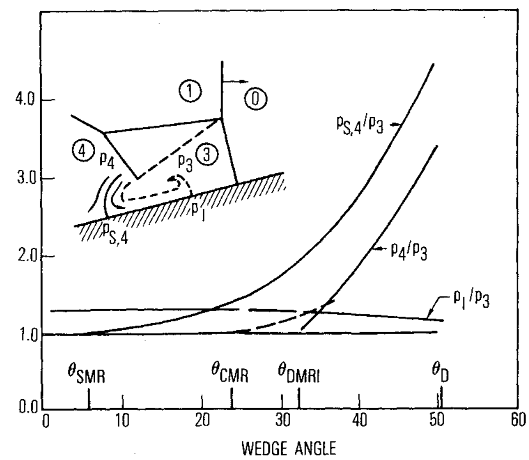

Fig. 7 Surface pressures in Mach reflection region, $\gamma = 7/5$.

transition from DMR to CMR to SMR, and the recirculation region (regions 4 and 5) are discussed herein.

Regions 1-3

The flow in regions 1-3 is a classical triple-point flow obtained subject to the assumptions that $p_2 = p_3$, u_2 and u_3 are parallel, and the primary Mach stem (denoted m in Fig. 3) is perpendicular to the wedge. Numerical results for regions 1-3 are presented in Table 3 for values of θ in the range $\theta \leq \theta_D$ (for which only a Mach reflection can exist).

It is seen in Table 3 that $M_2 > \bar{M}_2 > 1$ at $\theta = \theta_D$. The quantities M_2 and $\bar{M}_2$ denote the Mach number in region 2 relative to points T and E, respectively (e.g., Figs. 5a and 5b). Both M_2 and $\bar{M}_2$ decrease as θ decreases. The values of θ at which $\bar{M}_2 = 1$ and $M_2 = 1$ are noted in Table 2. The transition from double- to complex- to single-Mach reflection can be explained in terms of the variation of M_2 and $\bar{M}_2$ with a decrease in θ, from θ_D, as is discussed in the next section.

Transition Criteria

The second Mach stem m' (Fig. 3) is expected to occur near point E when $\bar{M}_2 > 1$. Hence, for values of θ near θ_D, a double-Mach reflection occurs with flows similar to those depected in Fig. 5. The location of the second Mach stem, near point E, is expected to persist, with a decrease in θ until a value of θ is reached at which $\bar{M}_2 = 1$. The value of θ corresponding to $\bar{M}_2 = 1$ is termed θ_{DMRI} herein and listed in Table 2 for several values of γ. The angle θ_{DMRI} is the lowest wedge angle at

Table 3 Mach reflection for the case of strong shock and ideal gas

	Region 1						Region 2				
γ	θ	ψ	M_I	β	$\frac{\rho_I}{\rho_0}$	$\frac{p_I}{M_i^2 p_0}$	M_2	δ	ω	$\frac{\rho_2}{\rho_I}$	$\frac{p_2}{p_I}$
7/5	50.030	3.165	3.054	7.108	6.000	1.167	2.320	14.506	16.835	2.013	2.778
	45.000	4.153	2.650	8.200	6.000	1.167	2.070	13.261	20.211	1.796	2.325
	40.000	5.214	2.316	9.393	6.000	1.167	1.850	11.906	24.126	1.624	1.998
	35.000	6.379	2.033	10.713	6.000	1.167	1.655	10.435	28.694	1.486	1.754
	30.000	7.678	1.792	12.178	6.000	1.167	1.484	8.852	34.035	1.375	1.568
	25.000	9.154	1.584	13.802	6.000	1.167	1.334	7.162	40.303	1.285	1.423
	20.000	10.864	1.407	15.582	6.000	1.167	1.208	5.388	47.674	1.211	1.309
	15.000	12.890	1.258	17.480	6.000	1.167	1.106	3.586	56.329	1.150	1.216
	10.000	15.345	1.139	19.386	6.000	1.167	1.033	1.888	66.377	1.097	1.139
	5.000	18.385	1.051	21.077	6.000	1.167	0.995	0.554	77.736	1.049	1.069
	1.000	21.370	1.007	22.046	6.000	1.167	0.995	0.025	87.505	1.010	1.014
5/3	54.660	2.513	2.809	9.162	4.000	1.250	1.823	16.223	21.228	1.972	3.396
	50.000	3.733	2.479	10.394	4.000	1.250	1.677	14.979	24.430	1.809	2.846
	45.000	5.111	2.186	11.802	4.000	1.250	1.535	13.514	28.357	1.661	2.412
	40.000	6.580	1.942	13.310	4.000	1.250	1.408	11.922	32.842	1.536	2.089
	35.000	8.168	1.737	14.924	4.000	1.250	1.295	10.215	37.941	1.432	1.842
	30.000	9.910	1.562	16.641	4.000	1.250	1.198	8.412	43.710	1.345	1.649
	25.000	11.849	1.413	18.448	4.000	1.250	1.116	6.547	50.196	1.271	1.496
	20.000	14.040	1.289	20.309	4.000	1.250	1.051	4.683	57.406	1.207	1.371
	15.000	16.547	1.186	22.157	4.000	1.250	1.004	2.922	65.277	1.151	1.265
	10.000	19.440	1.104	23.891	4.000	1.250	0.979	1.420	73.614	1.100	1.172
	5.000	22.775	1.043	25.392	4.000	1.250	0.977	0.379	82.043	1.051	1.086
	1.000	25.773	1.007	26.358	4.000	1.250	0.993	0.016	88.478	1.010	1.017

	Region 3					Region 4				
γ	θ	M_3	α	$\frac{\rho_3}{\rho_0}$	$\frac{p_3}{M_i^2 p_0}$	$\bar{M}_2$	$\frac{\rho_4}{\rho_2}$	$\frac{p_4}{p_2}$	$\frac{p_{s,4}}{p_3}$	$\frac{p_4}{p_I}$
7/5	50.030	0.398	71.644	6.000	3.241	1.755	2.287	3.427	4.466	9.519
	45.000	0.412	66.461	6.000	2.713	1.518	1.892	2.520	3.480	5.861
	40.000	0.431	61.299	6.000	2.331	1.301	1.517	1.807	2.716	3.612
	35.000	0.455	56.148	6.000	2.047	1.100	1.170	1.246	2.133	2.185
	30.000	0.486	51.030	6.000	1.829	0.914	1.000	1.000	1.716	1.568
	25.000	0.526	45.964	6.000	1.661	0.738	1.000	1.000	1.437	1.423
	20.000	0.576	40.971	6.000	1.527	0.574	1.000	1.000	1.250	1.309
	15.000	0.642	36.066	6.000	1.419	0.418	1.000	1.000	1.128	1.216
	10.000	0.728	31.273	6.000	1.328	0.270	1.000	1.000	1.052	1.139
	5.000	0.843	26.631	6.000	1.247	0.131	1.000	1.000	1.012	1.069
	1.000	0.965	23.071	6.000	1.183	0.026	1.000	1.000	1.000	1.014
5/3	54.660	0.454	80.045	4.000	4.245	1.185	1.276	1.506	2.598	5.113
	50.000	0.462	75.372	4.000	3.557	1.056	1.083	1.143	2.202	3.252
	45.000	0.475	70.316	4.000	3.015	0.923	1.000	1.000	1.868	2.412
	40.000	0.493	65.232	4.000	2.611	0.797	1.000	1.000	1.617	2.089
	35.000	0.516	60.138	4.000	2.302	0.678	1.000	1.000	1.428	1.842
	30.000	0.546	55.053	4.000	2.062	0.565	1.000	1.000	1.288	1.649
	25.000	0.584	49.995	4.000	1.870	0.458	1.000	1.000	1.184	1.496
	20.000	0.633	44.992	4.000	1.713	0.356	1.000	1.000	1.109	1.371
	15.000	0.695	40.079	4.000	1.582	0.259	1.000	1.000	1.057	1.265
	10.000	0.774	35.312	4.000	1.466	0.168	1.000	1.000	1.024	1.172
	5.000	0.874	30.771	4.000	1.357	0.081	1.000	1.000	1.006	1.086
	1.000	0.973	27.374	4.000	1.272	0.016	1.000	1.000	1.000	1.017

	Region 5					Interfaces				
γ	θ	$\bar{M}_5$	$\frac{\rho_5}{\rho_2}$	$\frac{\bar{u}_5}{u_i}$	$\frac{\tilde{u}_5}{u_i}$	$\frac{u_I}{\bar{u}_m}$	$\frac{p_I}{p_3}$	$\frac{\bar{u}_m}{u_i}$	$\frac{\bar{u}_w}{u_i}$	$\frac{\tilde{u}_w}{u_i}$
7/5	50.030	1.633	1.054	0.573	0.295	1.223	1.158	0.278	1.389	1.667
	45.000	1.463	1.023	0.596	0.342	1.350	1.194	0.254	1.271	1.525
	40.000	1.285	1.006	0.612	0.376	1.457	1.229	0.236	1.178	1.414
	35.000	1.099	1.000	0.618	0.397	1.538	1.257	0.221	1.104	1.324
	30.000	0.914	1.000	0.616	0.407	1.592	1.277	0.209	1.043	1.252
	25.000	0.738	1.000	0.610	0.411	1.630	1.292	0.199	0.994	1.193
	20.000	0.574	1.000	0.602	0.411	1.653	1.301	0.191	0.953	1.144
	15.000	0.418	1.000	0.592	0.408	1.666	1.306	0.184	0.919	1.103
	10.000	0.270	1.000	0.582	0.404	1.673	1.309	0.178	0.889	1.067
	5.000	0.131	1.000	0.571	0.399	1.677	1.311	0.172	0.862	1.034
	1.000	0.026	1.000	0.562	0.394	1.678	1.311	0.168	0.839	1.007
5/3	54.660	1.181	1.002	0.383	−0.078	0.486	1.040	0.461	1.382	1.843
	50.000	1.055	1.000	0.413	−0.009	0.561	1.053	0.422	1.265	1.687
	45.000	0.923	1.000	0.434	0.046	0.629	1.067	0.388	1.165	1.553
	40.000	0.797	1.000	0.447	0.086	0.685	1.080	0.361	1.084	1.445
	35.000	0.678	1.000	0.455	0.115	0.730	1.091	0.339	1.018	1.357
	30.000	0.565	1.000	0.458	0.137	0.765	1.101	0.321	0.963	1.284
	25.000	0.458	1.000	0.457	0.152	0.793	1.108	0.306	0.917	1.223
	20.000	0.356	1.000	0.455	0.162	0.814	1.114	0.293	0.878	1.171
	15.000	0.259	1.000	0.451	0.170	0.831	1.119	0.281	0.844	1.125
	10.000	0.168	1.000	0.447	0.176	0.845	1.123	0.271	0.812	1.083
	5.000	0.081	1.000	0.443	0.183	0.861	1.128	0.261	0.782	1.042
	1.000	0.016	1.000	0.441	0.189	0.877	1.133	0.252	0.756	1.009

which the second Mach stem remains near point E. With a further decrease in θ, $\bar{M}_2$ becomes subsonic while M_2 remains supersonic, and the second Mach stem moves toward point T. At some value of θ, termed θ_{CMR}, the second Mach stem is no longer apparent in interferograms and the transition to complex-Mach reflection is said to occur. At $\theta = \theta_{CMR}$ the flow Mach number in region 2, relative to the kink in the reflected wave (Fig. 1c), is sonic.[2,3] References 2 and 3 have proposed that the transition angle θ_{CMR} corresponds approximately to the Mach number condition $M_2 = 1.3$. Although this criterion is not well established, it has been used to determine the values of θ_{CMR} listed in Table 2. With a further decrease in θ, a value termed θ_{SMR} is reached at which $M_2 = 1$. The transition from CMR to SMR occurs at θ_{SMR} (see Table 2). The present results for critical angles agree with the results of Refs. 2 and 3 (for $\gamma = 7/5$ and $5/3$) and Ref. 4 (for $\gamma = 9/7$) in the limit of large values of M_i, except for the value of θ_{CMR} in Ref. 4. The latter value appears to correspond to $M_2 = 1.2$ rather than $M_2 = 1.3$, as noted in Fig. 2 and Table 2. All of the transition criteria, other than θ_{CMR}, are well established. The choice for θ_{CMR} probably requires further study.

Regions 4 and 5

Regions 4 and 5 are illustrated in Fig. 5c. Region 4 is the region downstream of the second Mach stem and region 5 is the recirculation region that results from the overpressure at stagnation point S. The evaluation of both the stagnation pressure $p_{s,4}$ and the characteristic velocity in region 5 (namely $\bar{u}_5$ in Fig. 5c) is a major objective of the present study. These quantities are evaluated in Appendix B by considering two regimes, namely $\bar{M}_2 \geq 1$ and $\bar{M}_2 < 1$. When $\bar{M}_2 \geq 1$ it is assumed that the second Mach stem is at point E and conditions in regions 2 and 4 are related by a shock of strength $\bar{M}_2$. When $\bar{M}_2 < 1$, it is assumed that the second shock stem, if it exists, is sufficiently weak that the pressure $p_{s,4}$ is isentropically related to conditions in region 2. In both cases ($\bar{M}_2 \geq 1$ and $\bar{M}_2 < 1$), the flow velocity in region 5 is found from an isentropic expansion from $p_{s,4}$ to the pressure $p_5 = p_2 = p_3$. Numerical results for $p_{s,4}$ and $\bar{u}_5$ are included in Table 3.

An estimate for the interface velocity $\bar{u}_I$ (Fig. 5c) is also obtained in Appendix B. The interface location

$$\frac{\mathrm{EI}}{\mathrm{EF}} = \frac{\bar{u}_I}{\bar{u}_m} \tag{2}$$

is included in Table 3 and plotted in Fig. 6. The present solution is self-consistent provided $\bar{u}_I/\bar{u}_m < 1$, since the primary shock has been assumed, in Appendix B, to be unperturbed by region 5. The latter assumption is satisfied for $\gamma = 5/3$ but is violated for $\gamma = 7/5$ and $9/7$. In the latter cases the recirculation region is expected to extend to the nominal primary Mach stem position and to accelerate and distort the Mach stem. Values of $\bar{u}_I/\bar{u}_m > 1$ are included in Table 3 and Fig. 6 to indicate the severity of the interaction between the recirculation region and the primary Mach stem. The interaction is seen to be more severe with a decrease in γ, as is observed experimentally.[4] An improved solution, for interface I location, is needed for those cases where the present theory indicates $\bar{u}_I/\bar{u}_m > 1$.

The point I, in Fig. 5c, is a local stagnation point in a coordinate system wherein point I is stationary. Estimates for the pressure at point I, namely p_I, are included in Table 3. (Values of p_I, corresponding to cases where $\bar{u}_I/\bar{u}_m > 1$, should be viewed as approximate.) It follows that the Mach reflection flowfield has two local surface-pressure maxima (p_I and $p_{s,4}$). These local maxima are consistent with experimental density contours.[4] The variation of the surface-pressure ratios $p_{s,4}/p_3$, p_4/p_3, and p_I/p_3 with wedge angle is illustrated in Fig. 7 for $\gamma = 7/5$. The ratios $p_{s,4}/p_3$ and p_4/p_3 have the values 4.5 and 3.4, respectively, at θ_D and decrease with wedge angle. The ratio p_I/p_3 remains near one for all values of wedge angle. Hence $p_{s,4}$ is the largest surface pressure in the Mach reflection region and occurs near point E.

Other properties of interest can also be deduced. For example, the Mach number of the flow in region 5, relative to the primary Mach stem m, is obtained from

$$\tilde{M}_5 = \bar{M}_5 \tilde{u}_5 / \bar{u}_5 \tag{3}$$

It is found that at θ_D, $\tilde{M}_5 = 1.28$, 0.84, and -0.24 for $\gamma = 9/7$, 7/5, and 5/3, respectively. The negative sign denotes velocity directed away from the Mach stem. Hence, for low values of γ (e.g., $\gamma = 9/7$), the flow in region 5 is supersonic relative to the primary Mach stem and may be decelerated near the interface I by a shock wave. An imbedded shock wave, near the upstream end of region 5 has, in fact, been observed in the numerical computations of Colella.[8]

Concluding Remarks

The present model assumes $M_i^2 \gg 1$ and, for an ideal gas, appears to give accurate results for $M_i \gtrsim 5$ (e.g., Fig. 2). Real gas effects are considered in Refs. 2 and 3 and might be approximated by use of an effective value of γ in the present model. This approach has not been explored. However, numerical computations by Needham[9] indicate that for the case of strong shocks in air, inclusion of a real gas equation of state increases the extent of region 5. This is in accord with the present results since the effective value of γ is reduced by real gas effects.

The triple-point trajectory angle ψ is deduced in Appendix D for the limiting case $\theta \to 0$ and M_i of arbitrary magnitude. It is shown that ψ decreases with a decrease in M_i, as expected from physical reasoning.

Appendix A: Strong Shock Relations

Let subscripts 1 and 2 denote (in the present section only) conditions upstream and downstream of a shock, and let subscripts n and t denote normal and transverse velocity components, respectively. Consider the case of an ideal gas with a large Mach number component normal to the shock, $M_n^{-2} \equiv (u_{n,1}/a_1)^{-2} < 1$. Conditions across the shock are then (e.g., Ref. 7)

$$\frac{\rho_2}{\rho_1} = \frac{u_{n,1}}{u_{n,2}} = K_1\left[1 + 0\left(\frac{M_n^{-2}}{\gamma - 1}\right)\right] \tag{A1a}$$

$$\frac{u_{t,1}}{u_{t,2}} = 1 \tag{A1b}$$

$$\frac{1}{M_n^2}\frac{p_2}{p_1} = K_2\left[1 + 0\left(\frac{M_n^{-2}}{(\gamma - 1)^{-1}}\right)\right]$$

$$\frac{1}{M_n^2}\frac{T_2}{T_1} \equiv \frac{1}{M_n^2}\left(\frac{a_2}{a_1}\right)^2 \tag{A1c}$$

$$\frac{1}{M_n^2}\frac{T_2}{T_1} = \frac{K_2}{K_1}\left[1 + 0\left(\frac{M_n^{-2}}{\gamma - 1}\right) + 0\left(\frac{M_n^{-2}}{(\gamma - 1)^{-1}}\right)\right] \tag{A1d}$$

where

$$K_1 = (\gamma + 1)/(\gamma - 1) \tag{A2a}$$

$$K_2 = 2\gamma/(\gamma + 1) \tag{A2b}$$

Appendix B: Mach Reflection

The Mach reflection associated with the passage of a planar shock wave over a wedge is considered herein for the case of a strong incident shock and an ideal gas. The flow is considered in coordinate systems wherein the points T, E, and F, respectively, (Fig. 5), are stationary.

Point T Stationary

The flow in regions 0-3 are steady-state flows in the coordinate system wherein the triple-point T is stationary (Fig. 5a). Flow velocity and Mach number are denoted as u and M, respectively. Dependent variables are found by the simultaneous solutions of equations relating the flow in regions 0-3. The wall and the fluid in region 0 have the same velocity, namely,

$$\frac{u_0}{u_1} \equiv \frac{u_w}{u_i} = \frac{1}{\cos(\theta+\psi)} \tag{B1}$$

Other quantities of interest are found as follows.

Region 1

Strong shock relations (Appendix A) indicate

$$\cot\beta = K_1 \tan(\theta+\psi) \tag{B2a}$$

$$\frac{u_1}{u_i} = \left(\frac{K_2}{K_1}\right)^{1/2} M_1 = \frac{1}{K_1 \sin\beta} \tag{B2b}$$

$$\frac{1}{K_2 M_i^2}\frac{p_i}{p_0} = \frac{K_1}{K_2 M_i^2}\frac{T_1}{T_0} = \frac{1}{K_1}\frac{\rho_1}{\rho_0} = 1 \tag{B2c}$$

Region 3

Again, from strong shock relations, $\rho_3/\rho_0 = K_1$ and

$$\tan\alpha = (\cot\psi)/K_1 \tag{B3a}$$

$$M_3 = [(1+K_1^2\tan^2\psi)/(K_1K_2)]^{1/2} \tag{B3b}$$

$$\frac{1}{K_2^2 M_i^2}\frac{p_3}{p_0} = \frac{K_1}{K_2 M_i^2}\frac{T_3}{T_0} = \left[\frac{\cos\psi}{\cos(\theta+\psi)}\right]^2 \tag{B3c}$$

$$\frac{u_3}{u_i} = \left(\frac{1}{M_i^2}\frac{T_3}{T_0}\right)^{1/2} M_3 \tag{B3d}$$

Region 2

The flow in region 2 corresponds to supersonic flow of Mach number M_1 over a wedge of half-angle δ defined by

$$\delta \equiv \alpha - \theta - \beta \tag{B4a}$$

Recall that $p_3 = p_2$ across the contact surface. It follows that

$$\xi \equiv \frac{p_2}{p_1} = \left(\frac{\cos\psi}{\cos(\theta+\psi)}\right)^2 \tag{B4b}$$

Oblique shock relations (e.g., Ref. 7) then indicate

$$\tan^2\delta = \left(\frac{K_1K_2M_1^2}{1+K_1\xi} - 1\right)\left(\frac{\xi-1}{\gamma M_1^2 - \xi + 1}\right)^2 \tag{B4c}$$

$$M_2^2 = \frac{M_1^2(K_1\xi+1) - [2/(\gamma-1)](\xi^2-1)}{\xi(\xi+K_1)} \tag{B4d}$$

$$\frac{T_2}{T_1} = \frac{\rho_1}{\rho_2}\xi = \frac{\xi(\xi+K_1)}{K_1\xi+1} \tag{B4e}$$

$$\frac{u_2}{u_i} = \frac{M_2}{M_1}\left(\frac{T_2}{T_1}\right)^{1/2}\frac{u_1}{u_i} \tag{B4f}$$

$$\omega = \left[\sin^{-1}\left(\frac{\xi+K_1}{K_1K_2\xi M_2^2}\right)\right]^{1/2} \tag{B4g}$$

Equations (B4c-f) correspond to the "weak" branch of the oblique shock solution. This may be confirmed by noting that $\xi \to 1$ as $\delta \to 0$ in Eq. (B4c). The weak solution is the one that generally occurs in physical flows.

Solution

Equations (B2a), (B2b), (B3a), and (B4a-c) provide six equations for the six dependent variables ψ, β, M_1, α, δ, and ξ. These equations define the flow in regions 0-3 and can be solved by trial and error after an initial estimate is made for ψ. Numerical results for dependent variables of interest are given in Table 1. The solution for region 4 is presented in the next section.

Point E Stationary

Point E is defined as the intersection between the contact surface (assumed uncurled) and the wall surface. When the flow in region 2 is supersonic, relative to E, a second Mach stem is generated (i.e., m' in Fig. 3) that nominally originates at point E. The flow in region 4 is steady when viewed in a coordinate system wherein point E is stationary. This coordinate system is illustrated in Figs. 5b and 5c. The flow depicted therein is now evaluated.

Flow velocity and Mach number in the point E stationary coordinate system are denoted by $\bar{u}$ and $\bar{M}$, respectively, and are obtained by subtracting the vector velocity $u_E = u_3$ in Fig. 5a from the velocities shown therein. Note that $\bar{u}_3 = 0$. The freestream, wall, and triple-point velocities are

$$\frac{\bar{u}_0}{u_i} \equiv \frac{\bar{u}_w}{u_i} = \frac{K_1-1}{K_1}\frac{\cos\psi}{\cos(\theta+\psi)} \tag{B5a}$$

$$\frac{\bar{u}_T}{u_i} \equiv \frac{1}{\cos(\alpha-\theta)}\frac{\bar{u}_i}{u_i} = \frac{1}{\sin\alpha}\frac{\bar{u}_m}{u_i} = \frac{u_3}{u_i} \tag{B5b}$$

The flow in region 2 is

$$\frac{\bar{u}_2}{u_i} = \frac{u_2}{u_i} - \frac{u_3}{u_i} \tag{B6a}$$

$$\bar{M}_2 = \left(M_i^2\frac{T_0}{T_1}\frac{T_1}{T_2}\right)^{1/2}\frac{\bar{u}_2}{u_i} \tag{B6b}$$

When $\bar{M}_2 > 1$, the second Mach stem m' (Fig. 3) may be assumed to originate in the vicinity of point E. Conditions in region 4 are then found from steady-state shock relations, namely,

$$\frac{p_4}{p_2} = \frac{2\gamma(\bar{M}_2)^2 - (\gamma-1)}{\gamma+1} \tag{B7a}$$

$$\frac{\bar{u}_2}{\bar{u}_4} = \frac{\rho_4}{\rho_2} = \frac{p_4}{p_2}\frac{T_2}{T_4} = \frac{(\gamma+1)(\bar{M}_2)^2}{(\gamma-1)(\bar{M}_2)^2+2} \tag{B7b}$$

$$\bar{M}_4 = \left[\frac{(\gamma-1)(\bar{M}_2)^2+2}{2\gamma(\bar{M}_2)^2-(\gamma-1)}\right]^{1/2} \tag{B7c}$$

$$\frac{p_{s,4}}{p_3} = \frac{p_{s,4}}{p_2} = \left[\frac{\gamma+1}{2}(\bar{M}_2)^2\right]^{\gamma/(\gamma-1)}\left(\frac{p_2}{p_4}\right)^{1/(\gamma-1)} \tag{B7d}$$

where $p_{s,4}$ is the pressure at the stagnation point S which develops in region 4 (Fig. 5c). When $\bar{M}_2 < 1$, the second Mach stem is assumed to be sufficiently weak so that the stagnation pressure at S is found from the isentropic relations

$$\frac{p_{s,4}}{p_3} = \frac{p_{s,4}}{p_2} = \left[1 + \frac{\gamma-1}{2}(\bar{M}_2)^2\right]^{\gamma/(\gamma-1)} \tag{B7e}$$

Equations (B7d) and (B7e) provide estimates of the maximum wall-surface pressure induced by the Mach reflection process and apply independently of the coordinate system. Since p_4 is larger than p_3 there will be an expansion of the flow from region 4 into region 3, as illustrated in Fig. 5c. The expanded flow is denoted region 5. The flow properties in region 5, corresponding to an isentropic expansion from region 4 to the pressure $p_5 = p_3 = p_2$, are (for $\bar{M}_2 > 1$)

$$(\bar{M}_5)^2 = \frac{2}{\gamma - 1}\left\{\left[1 + \frac{\gamma - 1}{2}(\bar{M}_4)^2\right]\left(\frac{p_4}{p_2}\right)^{(\gamma-1)/\gamma} - 1\right\} \tag{B8a}$$

$$\frac{T_5}{T_2} = \frac{\rho_2}{\rho_5} = \frac{1 + [(\gamma-1)/2](\bar{M}_5)^2}{1 + [(\gamma-1)/2](\bar{M}_2)^2} \tag{B8b}$$

$$\frac{\bar{u}_5}{u_i} = \frac{\bar{M}_5}{\bar{M}_2}\frac{\bar{u}_2}{u_i}\left(\frac{T_5}{T_2}\right)^{1/2} \tag{B8c}$$

When $\bar{M}_2 < 1$, re-expansion from the stagnation zone results in conditions in region 5 that are identical to those in region 2, except for the direction of flow. Thus, for $\bar{M}_2 < 1$

$$\frac{\bar{u}_5}{\bar{u}_2} = \frac{\bar{M}_5}{\bar{M}_2} = \frac{T_5}{T_2} = \frac{p_5}{p_2} = 1 \tag{B8d}$$

The location of the interface between regions 3 and 5, in the vicinity of the wall, is denoted I in Fig. 5. Point I represents a stagnation point between the flow in regions 3 and 5, when these flows are viewed in a point I stationary coordinate system. The static pressures, stagnation pressures, and Mach numbers relative to point I are equal in regions 3 and 5. It then follows that

$$\frac{\bar{u}_I}{u_i} = \frac{\bar{u}_5/u_i}{1 + (\rho_3/\rho_5)^{1/2}} \tag{B9a}$$

$$\frac{p_I}{p_3} = \left[1 + \frac{\gamma - 1}{2}\left(\frac{\bar{u}_I}{a_3}\right)^2\right]^{\gamma/(\gamma-1)} \tag{B9b}$$

where p_I is the local wall surface and $\bar{u}_I$ is the velocity of point I in point E stationary coordinates. Values of $\bar{u}_I$ and p_I are included in Table 3.

Point F Stationary

Point F is defined as the intersection between the primary Mach stem m and the wall surface (Fig. 3). The coordinate system considered herein assumes point F is stationary, whereas the freestream, wall, and triple point have motion. The present coordinate system is denoted by the tilde and is useful for analysis of the boundary layer in region 3.

Velocities in the F-stationary coordinate system are obtained by subtracting the Mach stem velocity $\bar{u}_m$ in the E-stationary system from velocities therein. The results are

$$\frac{\tilde{u}_w}{u_i} = \frac{\tilde{u}_0}{u_i} = \frac{\cos\psi}{\cos(\theta + \psi)} \tag{B10a}$$

$$\frac{\tilde{u}_E}{u_i} = \frac{\tilde{u}_3}{u_i} = \frac{1}{K_I}\frac{\cos\psi}{\cos(\theta + \psi)} \tag{B10b}$$

$$\frac{\tilde{u}_T}{u_i} = \frac{u_3}{u_i}\cos\alpha \tag{B10c}$$

$$\frac{\tilde{u}_2}{u_i} = \left[\left(\frac{\bar{u}_2}{u_i}\sin\alpha + \frac{\bar{u}_m}{u_i}\right)^2 + \left(\frac{\bar{u}_2}{u_i}\cos\alpha\right)^2\right]^{1/2} \tag{B10d}$$

$$\frac{\tilde{u}_4}{u_i} = \left[\left(\frac{\bar{u}_4}{u_i}\sin\alpha + \frac{\bar{u}_m}{u_i}\right)^2 + \left(\frac{\bar{u}_4}{u_i}\cos\alpha\right)^2\right]^{1/2} \tag{B10e}$$

$$\frac{\tilde{u}_5}{u_i} = \frac{\bar{u}_5}{u_i} - \frac{\bar{u}_m}{u_i} \tag{B10f}$$

Values are listed in Table 3.

Appendix C: Regular Reflection

The flowfield in regions 0-2 is evaluated herein for the case of a strong incident shock and regular reflection. The coordinate system considered is the one wherein point T (now a point of regular reflection) is stationary (Fig. 3).

The equations derived in Appendix B for regions 0-2 are applicable, subject to the boundary condition that the flow in region 2 be tangent to the wedge surface. The angle α is now viewed as the angle between the streamlines in region 2 and the normal to the wedge surface. It follows that

$$\alpha = \pi/2 \tag{C1a}$$

$$\delta = (\pi/2) - \theta - \beta \tag{C1b}$$

For given values of γ and θ, the quantities β and M_I are found from Eqs. (B2). The pressure ratio ξ is then found from Eq. (B4c) by iteration, and all other quantities of interest can be evaluated from expressions for regions 1 and 2 in Appendix B. [Note that Eq. (B4b) is not applicable.] Numerical results are presented in Table 2. The minimum value of θ therein corresponds to the condition for oblique shock detachment from the equivalent wedge δ. The latter value of θ is denoted θ_D and is usually considered the value of θ at which the transition from regular to Mach reflection occurs. Values of θ_D are found by replacing Eq. (B4c) by the shock detachment condition (e.g., Ref. 7)

$$\xi = \frac{(\gamma+1)(M_I^2 - 2) + \{(\gamma+1)[(\gamma+1)M_I^4 + 8(\gamma-1)M_I^2 + 16]\}^{1/2}}{2(\gamma+1)} \tag{C2}$$

and are given in Table 2.

Appendix D: Limit Solution

The triple-point trajectory angle ψ is evaluated in the limit $\theta \to 0$ for cases of arbitrary shock strength M_i.

Let t denote the time elapsed since the shock reached the wedge leading edge. In this time, the shock has moved a distance $u_i t$. A cylindrical acoustic wave, generated at $t = 0$, now has a radius $a_I t$ centered a distance $u_I t$ downstream of the leading edge. The intersection of the cylindrical wave with the incident shock defines the triple-point location. The result, using shock relations from Ref. 7, is

$$\tan\psi = \left[\frac{\gamma - 1}{\gamma + 1}\left(1 - \frac{1}{M_i^2}\right)\left(1 + \frac{2}{(\gamma+1)M_i^2}\right)\right]^{1/2} \tag{D1a}$$

$$\tan\psi = [2(M_i - 1)]^{1/2} \qquad M_i \to 1 \tag{D1b}$$

$$\tan\psi = \left[\frac{\gamma - 1}{\gamma + 1}\right]^{1/2} \qquad M_i \to \infty \tag{D1c}$$

It is seen that ψ decreases as M_i (i.e., a_I) decreases, as is expected from physical reasoning. For $M_i^2 \gg 1$ Eq. (D1a) indicates $\psi = 19.47$, 22.21, and 26.57 when $\gamma = 9/7$, 7/5, and 5/3, respectively. These results are consistent with the data in Table 3.

Acknowledgments

This work was partially supported by Defense Nuclear Agency (DNA) under Air Force Space Division Contract F04701-82-C-0083. The computational support of Karen Foster is gratefully acknowledged.

References

[1]Bazhenova, T. V., Fokeev, V. P., and Gvozdeva, L. G., "Regions of Various Forms of Mach Reflection and Its Transition to Regular Reflection," *Acta Astronautica*, Vol. 3, 1976, p. 131.

[2]Ben-Dor, G. and Glass, I. I., "Domains and Boundaries of Non-Stationary Oblique Shock-Wave Reflexions. 1. Diatomic Gas," *Journal of Fluid Mechanics*, Vol. 92, 1979, p. 459.

[3]Ben-Dor, G. and Glass, I. I., "Domains and Boundaries of Non-Stationary Oblique Shock-Wave Reflexions. 2. Monatomic Gas," *Journal of Fluid Mechanics*, Vol. 96, 1980, p. 735.

[4]Ando, S. and Glass, I. I., "Domains and Boundaries of Pseudostationary Oblique Shock-Wave Reflections in Carbon Dioxide," Seventh International Symposium on Military Applications of Blast Simulation, Medicine Hat, Canada, July 1981.

[5]Fry, M., Picone, J. M., Boris, J. P., and Book, D. L., "Transition to Double-Mach Stem for Nuclear Explosion at 104-ft Height of Burst," NRL MR 4630, Nov. 17, 1981.

[6]Mirels, H., "Mach Reflection Flow Fields Associated with Strong Shocks," Aerospace Corp., El Segundo, Calif., TR-0083(3785)-1, 1983.

[7]"Equations, Tables, and Charts for Compressible Flow," NACA Rept. 1135, 1953.

[8]Collela, P., private communication, Lawrence Berkeley Lab., Berkeley, Calif.

[9]Needham, C. E., private communication, S-Cubed Corp., Albuquerque, N. Mex.